Fluid Dynamics & Materials Processing
DOI:10.32604/fdmp.2020.010545
Article

Tech Science Press

Microscopic Simulation of Expansive Soils and Evolution Laws

Lin Pan, Jinhong Xia and Hongxing Han*

School of Civil Engineering and Architecture, Xinxiang University, Xinxiang, 453003, China
*Corresponding Author: Hongxing Han. Email: hxhan@whu.edu.cn
Received: 09 March 2020; Accepted: 22 September 2020

Abstract: In this paper, the discrete element method (DEM) is used to study the microstructure of expansive soils. The results of the numerical calculations are in agreement with the stress-strain triaxial test curve that is obtained for a representative expansive soil. Biaxial compression tests are conducted for different confining pressures (50 kpa, 100 kpa, and 150 kpa). Attention is paid to the following aspects: deviatoric stress, boundary energy, friction energy, bond energy, strain energy, kinetic energy, and the contact force between grains when the test specimen is strained and to the effect of the different confining pressures on the internal crack expansion. The results of this research show that the cross-section of the specimen is destroyed along the middle part of the specimen itself. When the confining pressure is higher, the impulse is stronger, and this leads to more effective destruction.

Keywords: Expansive soil; particle flow; parallel-bond; crack

1 Introduction

At present, road, railway, bridge, and other projects have developed rapidly in the world, and the requirements for structures are increasingly strict. If the foundation works are not properly treated, the superstructure will be damaged, and this causes problems such as great harm to building construction, train noise [1–3], and foundation settlement [4–6]. In the field of geotechnical engineering, a lot of research has been conducted on the characteristics of multiple fractures in expansive soil. Rosenbalm et al. [7] studied the variation law of the expansion rate of expansive soil under different overburden loads, different initial moisture contents, dry and wet cycle times, and dry density. Cao et al. [8] studied the evolution of expansive soil fissures under rainfall-evaporation conditions and reported that the dehumidification process was divided into three stages: A slow phase, fast phase, and slow growth phase. Han et al. [9] used indoor simulated expansive soil as a research object, analyzing the cracking characteristics of soil under the condition of a dry-wet cycle and the effect of fiber reinforcement on the development of cracks. Xu et al. [10] carried out an experimental study on remolded expansive soil in Nanyang. They found that the dehumidification cracking process was divided into three stages: The crack initiation stage, fracture generation stage, and stabilization stage. Morris et al. [11] established the theoretical relationship among crack depth, soil characteristics, and suction distribution, and they proposed three methods to predict soil cracking depth. Li et al. [12] used digital photography to obtain fracture images of expansive soil and quantitatively studied the effect of cracks on the engineering characteristics of expansive soil. Hu et al. [13] used Matlab software and wrote a program to reconstruct

a CT image and to extract the fracture information. It was found that crack development begins at the initial microcracks and holes in the soil and gradually expands, finally forming a through fracture surface. Tan et al. [14] conducted simulation experiments using PFC3D software, and they verified that crack development was the main reason for the attenuation of expansive soil. To date, some valuable results have been obtained from studies of cracks in expansive soil, but most of the results are qualitative and have rarely involved the propagation of cracks in expansive soil. In this paper, expansive soil was simulated using two-dimensional particle flow (PFC2D) software. This paper provides reference to theoretical research and engineering of expansive soil.

The idea of the discrete element method (DEM) stems from earlier molecular dynamics. It was first proposed by Cundall in 1971 and applied to geotechnical engineering [15]. Particle flow is a DEM that uses discs or circles. The particle unit simulates the motion and interaction of a circular granular medium. This method overcomes the problems that are caused by the macroscopic assumptions of the traditional continuum model. It not necessary to specify the constitutive relationship; only Newton's second law and the relationship between force and displacement need to be calculated. The engineering properties of geomaterials are simulated from a microscopic point of view, and these two laws let the balls and contacts translate force and moment and different deformations caused by them. The macroscopic mechanical behavior of materials is analyzed by studying various mesoscopic parameters. In recent years, the research of domestic and foreign scholars on noncontinuous dielectric materials has mainly been represented by PFC2D/PFC3D software, which was developed by American ITASCA. At present, particle DEM is widely applied in geotechnical, mining, dynamic impact, and other fields [16–20], and it is becoming an effective tool for studying mechanical properties of granular media.

2 Basic Theory of Two-Dimensional Particle Flow

2.1 Basic Assumption of Particle Flow

Two-dimensional particle flow makes the following assumptions during the simulation: (1) The particle unit is a disc or a sphere. (2) The particle is a rigid body. (3) The particle contact is a flexible contact, and the contact has a certain amount of overlap. The size of the "overlap amount" is related to the contact force, and the "overlap amount" is small compared with the particle size. (4) Particle contact occurs over a small range. (5) There is a special connection strength at the contact. The calculation method of particle flow is mainly based on the relationship between Newton's second law and force-displacement. The calculation principle uses the central difference method for dynamic relaxation. The motion between particles is considered to be a dynamic process of change, and the internal force automatically goes to the equilibrium state at each time step.

2.2 Parallel Bonding Model

The parallel bond model is a constitutive relationship that describes a cemented material in a limited range between particles, and this material can hinder slipping between particles. The parallel bond model assumes that there is a series of springs whose normal stiffness and tangential stiffness are constant on a circular or rectangular plane centered on the indirect contact of the particles. The springs are divided into contact springs and parallel bonded springs. The relative motion of the contact points between particles generates forces and torques. If any of the maximum stresses exceeds the corresponding ultimate strength, the parallel connection breaks.

The parallel bond model has five parameters: Stiffness ($\bar{k}^n$), tangential stiffness ($\bar{k}^s$), normal strength ($\bar{\sigma}_c$), tangential strength ($\bar{\tau}_c$), and bond radius ($\bar{R}$). These parameters can be used with the properties commands pb_kn, pb_ks, pb_nstrength, pb_sstrength and pb_radius. The forces ($\bar{F}_i$) and moments ($\bar{M}_i$) that act on the parallel connections are decomposed into normal components ($\bar{F}_i, \bar{M}_i$) and tangential components ($\bar{F}_i^s, \bar{M}_i^s$).

Fig. 1 shows that when the bond is formed, the parallel connection force and torque are initialized to zero. As the load is applied, the relative displacement between the particles and the increase in the angle results in an increase in the relative force and moment, respectively. The changes in force and torque are expressed as follows:

$$\begin{cases} \Delta\bar{F}_i^n = \left(-\bar{k}^n A \Delta U^n\right) n_i \\ \Delta\bar{F}_i^s = -\bar{k}^s A \Delta U_i^s \\ \Delta U_i = V_i \Delta t \end{cases} \tag{1}$$

$$\begin{cases} \Delta\bar{M}_i = -\bar{k}^n I \Delta\theta_i \\ \Delta\theta = \left(\omega_i^{[B]} - \omega_i^{[A]}\right) \Delta t \end{cases} \tag{2}$$

where A stands for the area of the disc, $\bar{R}$ is the radius of the disc, and I is the moment of inertia of the cross-section against the rotation direction along the contact point. The vector of force and moment in the new moment is the superposition of the force and moment that are generated by the contact position in the past moment. The force and torque vectors at the new moment are as follows:

$$\begin{cases} \bar{F}_{i+1}^s = \bar{F}_i^s + \Delta\bar{F}_i^s \\ \bar{F}_{i+1}^n = \bar{F}_i^n + \Delta\bar{F}_i^n \\ \bar{M}_{i+1} = \bar{M}_i + \Delta\bar{M}_i \end{cases} \tag{3}$$

According to the beam formula, the maximum tensile stress and maximum shear stress at the edge of the beam are obtained as follows:

$$\begin{cases} \sigma_{\max} = \dfrac{-\bar{F}_i^n}{A} + \dfrac{\left|\bar{M}_i^s\right|}{I}\bar{R} \\ \tau_{\max} = \dfrac{\left|\bar{F}_i^s\right|}{A} + \dfrac{\left|\bar{M}_i^s\right|}{J}\bar{R} \end{cases} \tag{4}$$

where J is the polar moment of inertia of the section. If the maximum normal stress is greater than the normal strength ($\sigma_{\max} > \sigma$) or if the maximum tangential stress is greater than the tangential strength ($\tau_{\max} > \tau$), then the parallel connections between particles are destroyed. Otherwise, forces and moments are transferred between adjacent particles.

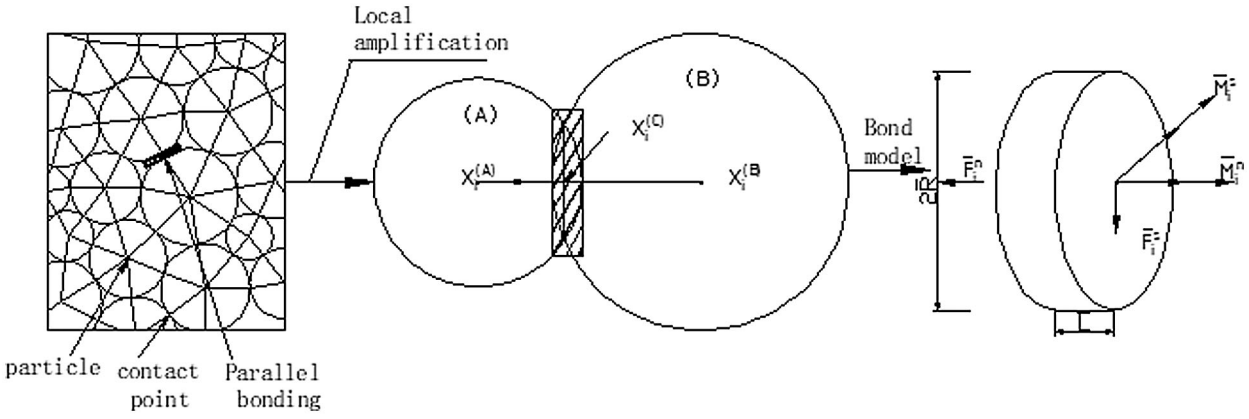

Figure 1: Parallel model

3 Numerical Simulation of Particle Flow in a Biaxial Test of Expansive Soil

3.1 Established Model of Expansive Soil

According to the standard for the indoor triaxial test specimen model with $h = 200\,mm$ and $D = 101\,mm$, four walls of the model that are 1.2 times of the height and width of the specimen are created. A coordinate system is also established. The stiffness, friction coefficient, joint strength, density, and particle contact modulus of the wall and sphere are defined. To eliminate the anisotropy of particles that are the same size, the generated particle radius is uniformly distributed by $R_{\min} \sim R_{\max}$, and the average radius r is $(R_{\min} \sim R_{\max})/2$, where $R_{\min} = 0.75$ and $R_{\max} = 2.1$. The number of particles produced is 2,659, which meets the accuracy and quantitative requirements of the calculation.

3.2 Verification of Numerical Simulation

According to the macroscopic parameters of the indoor triaxial test (elastic modulus, peak strength, and shear strength), combined with the relationship between the macroscopic and microscopic mechanical parameters of the parallel-bond contact model adopted by Yang et al. [21], the mesoscopic parameters were constantly adjusted and a comparison was made with the indoor triaxial stress strain curve of typical expansive soil [22]. As shown in Fig. 2, the PFC2D simulation of the stress and strain curve and the change of the stress-strain curves for the indoor triaxial test are consistent for similar strengths, and this shows that the selection of mesoscopic parameters reflects the basic mechanical properties of expansive soil. The microscopic parameters are shown in Tab. 1. It can be seen from the entire picture that the curve of numerical simulation fluctuates little, as the influence of particle breakage is not considered in the numerical model. Xu et al. [23] showed that the particle crushing degree would also increase with an increase in the confining pressure. Therefore, the values of confining pressure that are used for numerical simulation in this paper are 50 kPa, 100 kPa, and 150 kPa.

Table 1: Microscopic parameters

Sample size/mm	Friction coefficient	Particle contact modulus/Pa	Parallel bond modulus/Pa	Parallel bond stiffness ratio
200 × 101	0.30	14×10^6	12×10^6	1.5

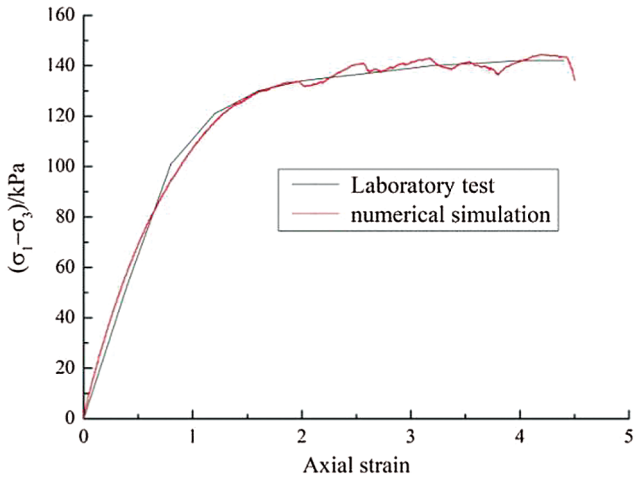

Figure 2: Stress-strain curve

4 Results and Analysis

4.1 Mechanical Behavior

The stress-strain curves under different values of confining pressure are shown in Fig. 3. As seen in Fig. 3, the peak strength of the stress-strain curve increases with an increase in the confining pressure. Meanwhile, the axial strain that corresponds to the peak strength achieved with low confining pressure is less than that which corresponds to the peak strength achieved with high confining pressure. When the confining pressure reached a peak point of 50 kPa, the stress-strain curve showed a strain softening phenomenon. When the curves for confining pressures of 100 kPa and 150 kPa reached their peaks, they showed a strain hardening trend. These results are consistent with the trend of expansive soil, which softens with low confining pressures and hardens with high confining pressures. Therefore, the microscopic parameters of DEM that are used in this paper can well describe the macroscopic mechanical characteristics of expansive soil materials.

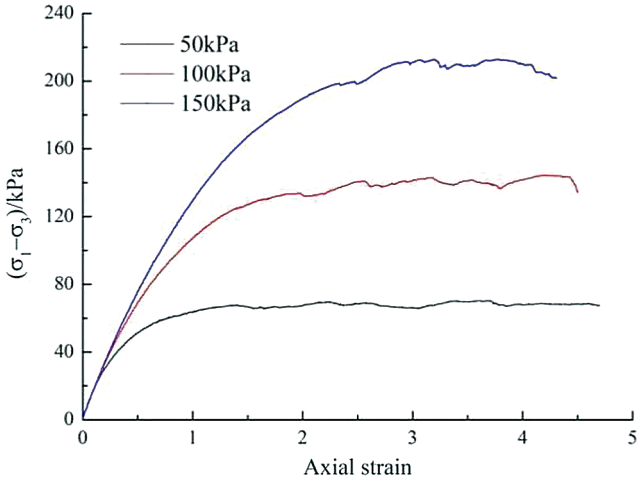

Figure 3: Deviator stress and axial strain

4.2 Crack Growth

A crack indicates a failure of the bond strength between two particles, and a tensile crack indicates a situation where the fracture direction of two adjacent particles is parallel to the direction of the load. A shear crack indicates the case where the direction of the fracture is perpendicular to the direction of the load. As seen in Fig. 4, when the axial strain increases, the total number of cracks increases sharply at first, and then it increases slowly and tends to be constant at end. Under the same confining pressure, the number of shear cracks is much larger than that of tensile cracks, and this indicates that the biaxial compression test is mainly caused by shear failure. Under the same axial strain, the number of total cracks that occur with low confining pressure was larger than that with a high confining pressure. The reason for this is that the increase in confining pressure causes a significant degree of compression densification on the specimen; also, the specimen was not easily destroyed, and this led to a relative decrease in the number of total cracks.

4.3 Contact Force of Particles

As seen in Fig. 5, the black rectangle represents the parallel contact force between particles. When the rectangular area is larger, the contact force is greater. Larger contact should be mainly distributed near the pressure plate. During the loading process, the contact force is gradually destroyed, and internal damage is the most obvious. With an increase in the axial displacement, the deviatoric stress increases gradually.

When stress concentration occurs in a certain area, contact forces among a large number of particles are destroyed, and a macroscopic shear fault zone form. The failure of specimens is transmitted along the central boundary of the model to both ends. This is consistent with the failure condition of the triaxial test specimen in the laboratory, and the occurrence of microcracks is accompanied by deviatoric stress, which reaches a certain value. The short red curve represents shear cracks, and the short black curve represents tensile cracks. The number of shear cracks is much larger than that of tensile cracks, and this indicates that shear failure is the main cause of the biaxial compression test.

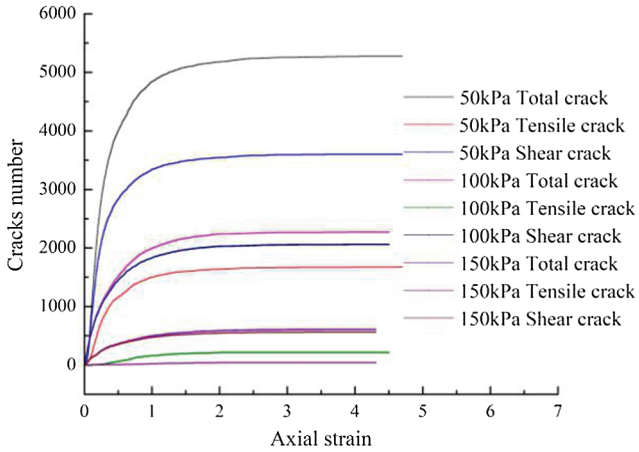

Figure 4: Number of cracks and axial strain

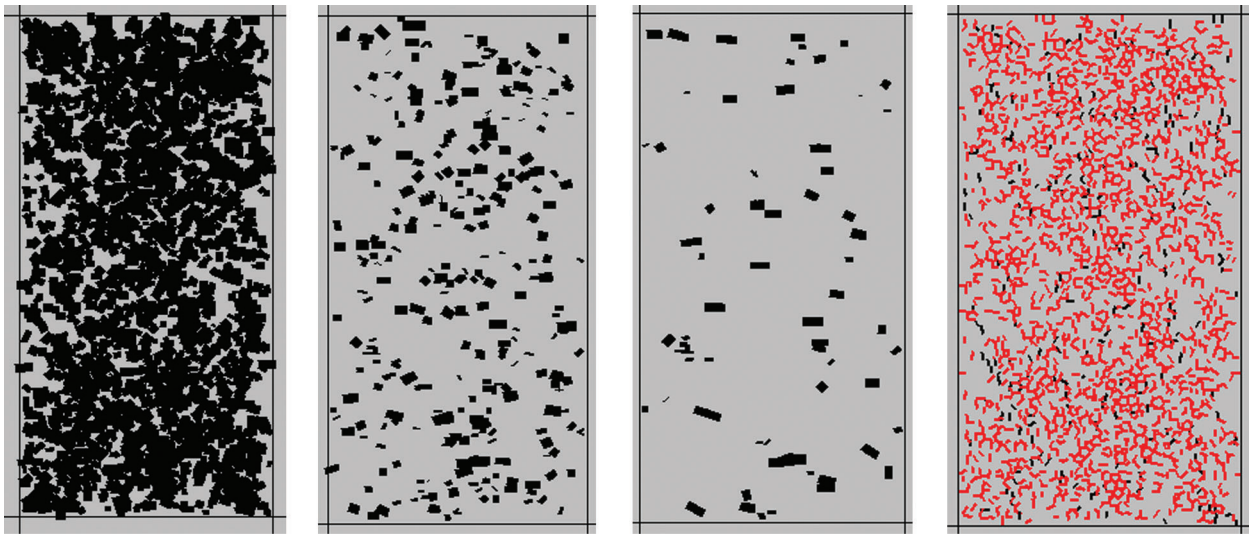

Figure 5: Contact force changes. (a) Before loading (b) Loading (c) Failure (d) End of loading

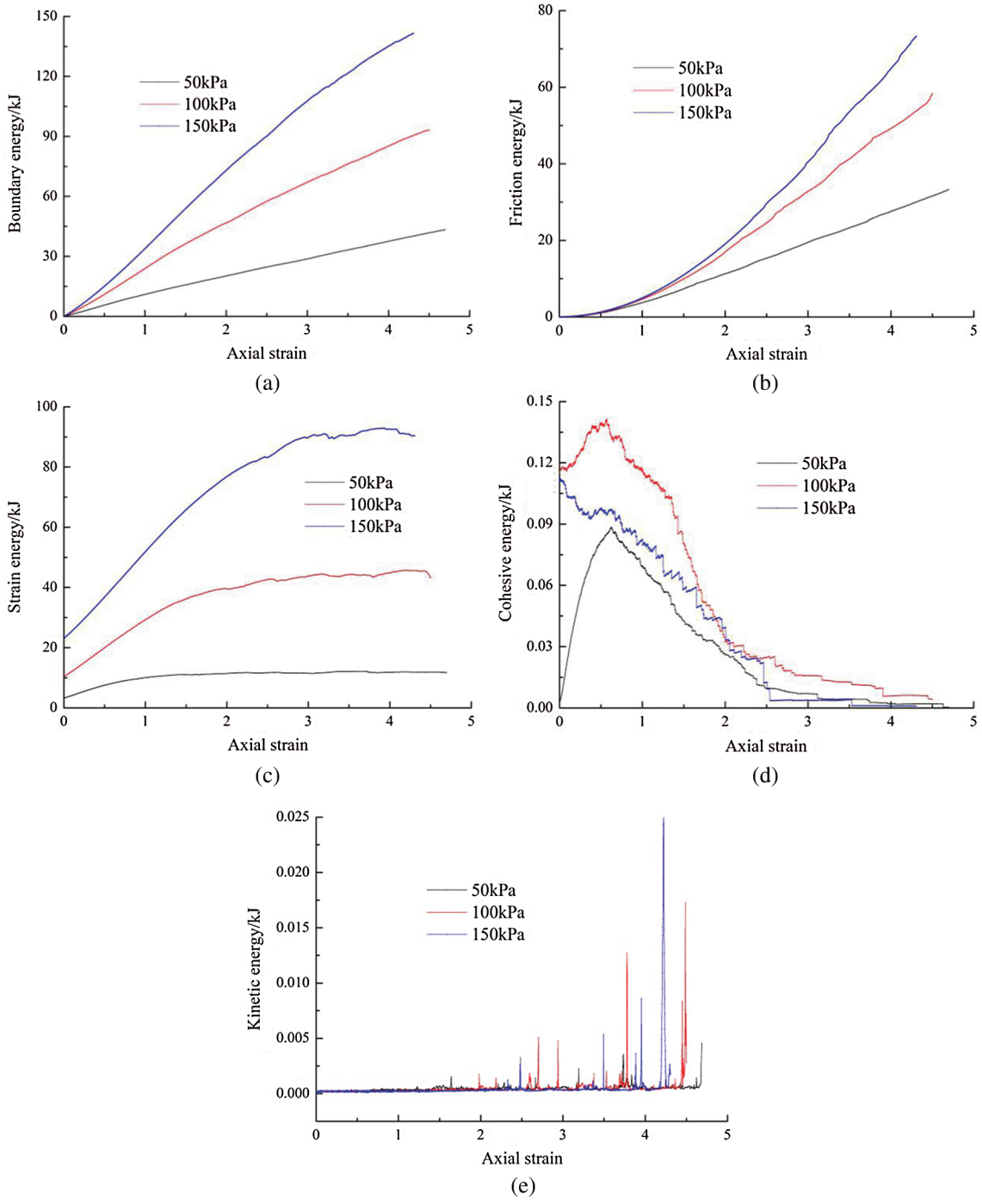

Figure 6: Energy and axial strain. (a) Boundary energy and axial strain (b) Friction energy and axial strain (c) Strain energy and axial strain (d) Bond energy and axial strain and (e) Kinetic energy and axial strain

4.4 Energy Evolution

It is not enough only to observe the failure mechanism of expansive soil from the macroscopic failure state and the mechanical properties of stress-strain curves. For an energy perspective, this paper analyzes the

transformation of energy in the loading process of the specimen and the adjustment of various energies in the loading process. It also explains the main role of various energies in the failure process of the specimen, and this is of certain reference value for studying the properties of expansive soil materials.

As seen in Figs. 6a–6c, the boundary energy, friction energy, and strain energy of the three confining pressures gradually increase with an increase in the axial strain. With the same axial strain, the three energy values that correspond to the high confining pressure are larger than those that correspond to the low confining pressure. The reason for this is that the high confining pressure generates a large external force, and this increases the boundary energy and friction energy. When the confining pressure is higher, a larger strain energy is required for specimen failure, and thus, the soil sample is less likely to be destroyed. At the same time, a higher confining pressure increases the density of particles in the sample. Also, the number of contacts between the particles increases, and this results an increase in the strain energy. Meanwhile, the specimen particles have a certain strain energy in the isotropic consolidation stage. As seen in Fig. 6d, when the confining pressure is 50 kPa and 100 kPa, the bonding energy in the elastic phase increases rapidly with an increase in the axial strain. Then, the particle bonds rupture at the peak point, and this results in a rapid decrease in the bonding energy. When the confining pressure is 150 kpa, the bonding energy decreases with an increase in the axial strain, and this indicates that the bonding energy of the confining pressure reaches the maximum in the isoconsolidation stage of the test piece. Also, the maximum bonding energy value of the three confining pressures happens in the elastic phase. Values occur during the elastic deformation phase. As seen in Fig. 6e, several specimens experience multiple pulses before failure under three confining pressures, and this indicates that the failure of the specimen is unstable. Also, the maximum pulse value is positively proportional to the confining pressure; the pulse value of the test piece is the largest at the point of failure under the same confining pressure, and the particle position adjusts to the maximum at this moment.

5 Conclusions

1. The evolution law of strain energy for typical expansive soil is consistent with the change law of the stress-strain curve. The evolution law of strain energy is the underlying reason for the macroscopic mechanical performance of soil.
2. A crack increases rapidly with an increase in the axial strain. Then, it increases slowly, and finally stabilizes. The number of shear cracks is greater than the number of cracks, and the biaxial compression test is mainly based on shear stress. When the confining pressure is higher, the number of cracks is less, and the high confining pressure inhibits damage to the specimen.
3. The contact stress is the largest in the vicinity of the pressure plate, and the damage from contact stress is accompanied by the generation of cracks. When stress concentration occurs in a certain area, a large amount of contact stress is destroyed, and macroscopic shear surface forms. The penetration form of the internal crack in the test piece is consistent with the sectional form of the indoor triaxial test piece.
4. In the parallel bond model, deviatoric stress, boundary energy, frictional energy, and strain energy increase with an increase in the axial strain, and the value of the corresponding confining pressure is greater than that of the corresponding lower confining pressure. The maximum binding energy of the three confining pressures occurs in the elastic phase, but the storage phase of the bonding energy is slightly different. The damage of the test piece is unstable. When the confining pressure is higher, the pulse value is larger, and the damage to the test piece is more severe.

Acknowledgement: This paper is under the support of Jinhong Xia team of Xinxiang University.

Funding Statement: This work is financially supported by the National Science Foundation of China (41877251) and the science and technology innovation fund project of Xinxiang University (15ZA06).

Conflicts of Interest: The authors declare that they have no conflicts of interest to report regarding the present study.

References

1. Zhang, X. H., Jiang, Y., Li, T. (2020). Effect of streamlined nose length on the aerodynamic performance of a 800 km/h evacuated tube train. *Fluid Dynamics & Materials Processing, 16(1),* 67–76. DOI 10.32604/fdmp.2020.07776.
2. Shen, D. M., Si, H., Xia, J. H., Li, S. Q. (2019). A new model for the characterization of frozen soil and related latent heat effects for the improvement of ground freezing techniques and its experimental verification. *Fluid Dynamics & Materials Processing, 15(1),* 63–76. DOI 10.32604/fdmp.2019.04799.
3. Liu, J. l., Yu, M. G., Chen, D. W., Yang, Z. G. (2020). A study on the reduction of the aerodynamic drag and noise generated by the roof air conditioner of high-speed trains. *Fluid Dynamics & Materials Processing, 16(1),* 21–30. DOI 10.32604/fdmp.2020.07658.
4. Yuan, S., Liu, X., Sloan, S. W. (2016). Multi-scale characterization of swelling behaviour of compacted Maryland clay. *Acta Geotechnica, 11(4),* 789–804. DOI 10.1007/s11440-016-0457-5.
5. Cheng, Z. L., Gong, B. W., Hu, B. (2015). Strength and test method of expansive soil. *Journal of Geotechnical Engineering, 37(S1),* 11–15.
6. Zhang, R., Zhang, B. Y., Zheng, J. L., Liu, Z. N. (2018). Modified lateral confined swelling tests on expansive soils. *Chinese Journal of Geotechnical Engineering, 40(12),* 2223–2230.
7. Rosenbalm, D., Zapata, C. E. (2016). Effect of wetting and drying cycles on the behavior of compacted expansive soils. *Journal of Materials in Civil Engineering, 29(1),* 04016191. DOI 10.1061/(ASCE)MT.1943-5533.0001689.
8. Cao, L., Wang, Z. J., Zhang, Z. H. (2016). Experimental study on fracture evolution characteristics of expansive soil under rainfall evaporation condition. *Journal of Rock Mechanics and Engineering, 35(2),* 413–421.
9. Han, C. P., Tian, J. Y., Zhang, J., Li, J. H. (2019). Analysis of fracture characteristics of fiber reinforced expansive soil under dry wet cycle. *Journal of Jilin University (Engineering and Technology Edition), 49(2),* 392–400.
10. Xu, X. C., Zhou, W., Chen, S. X. (2015). Fracture cracking characteristics and influencing factors of expansive soil in the whole process of dehumidification in Nanyang remodeling. *Geotechnical Mechanics, 36(9),* 2569–2584.
11. Morris, P. H., Graham, J., Wlliams, D. J. (1992). Cracking in drying soils. *Canadian Geotechnical Journal, 29(2),* 262–277. DOI 10.1139/t92-030.
12. Li, W., Liu, G. S., Yao, T. (2014). Improvement of image processing and feature extraction method of expansive soil fissures. *Geotechnical Mechanics, 35(12),* 3619–3626.
13. Hu, X. D., Li, X., Zhou, C. Y., Xue, L., Liu, H. F. et al. (2018). Quantitative analysis of cyclic expansion and contraction cracks of expansive soil. *Rock and Soil Mechanics, 39(S1),* 318–324.
14. Tan, B., Zheng, J. L., Zhang, R. (2014). Study on strength law of expansive soil crack based on laboratory test and numerical simulation. *Journal of Applied Mechanics, 31(3),* 463–467.
15. Cundall, P. A. (1971). A computer model for simulating progressive large scale movements in blocky system. In: MullerL (eds.), *Proceedings of the International Symposium on Rock Mechanics*, pp. 8–12, Rotterdam: A. A. Balkema.
16. Itasca Consulting Group, Inc. (2008). *The manuals of Particle Flow Code in 2-Dimension*. Version 3.1. Minneapolis.
17. Zhou, J., Bai, Y. F., Zhang, Z., Jia, M. C. (2009). Lab model tests and PFC2D modeling of pile groups in sands. *Chinese Journal of Geotechnical Engineering, 8,* 1275–1280.
18. Zhou, Z., Xing, K., Yao, H., Yang, H., Wang , H. (2019). Damage mechanism of soil-rock mixture after freeze-thaw cycles. *Journal of Central South University, 26(1),* 13–24. DOI 10.1007/s11771-019-3979-9.

19. Chen, H. Y., Yamamoto, H., Thoeni, K., Wu, Y. (2017). An analytical solution for geotextile-wrapped soil based on insights from DEM analysis. *Geotextiles and Geomembranes, 45(4),* 361–376. DOI 10.1016/j.geotexmem.2017.05.001.
20. Zheng, L. N., Xie, Q., Zhao, W., Qu , M. F., Li , C. H. (2011). Microscopic mechanics of debris accumulation body with expansive fine grain and PFC numerical simulation. *Advanced Materials Research, 249,* 4188–4194. DOI 10.4028/www.scientific.net/AMR.243-249.4188.
21. Yang, B. D., Jiao, Y., Lei, S. T. (2006). A study on the effects of microparameters on macro-properties for specimen created by bond particle. *Engineering Computations, 23(6),* 607–631. DOI 10.1108/02644400610680333.
22. Lu, Z. H., Chen, Z. H., Sun, S. G. (2002). Study on deformation and strength characteristic of expansive soil with triaxial tests. *Chinese Journal of Rock Mechanics and Engineering, 21(5),* 717–723.
23. Xu, M., Hong, J., Song, E. (2017). DEM study on the effect of particle breakage on the macro- and micro-behavior of rockfill sheared along different stress. *Computers and Geotechnics, 89,* 113–127. DOI 10.1016/j.compgeo.2017.04.012.